Chapter from:
Clouds in the Perturbed Climate System, edited by Jost Heintzenberg and Robert J. Charlson.
2009. Strüngmann Forum Report, vol. 2. Cambridge, MA: MIT Press. ISBN 978-0-262-01287-4

17

What Do We Know about Large-scale Changes of Aerosols, Clouds, and the Radiation Budget?

Teruyuki Nakajima[1] and Michael Schulz[2]

[1] Center for Climate System Research, University of Tokyo, Kashiwa, Chiba, Japan
[2] Laboratoire des Sciences du Climat et de l'Environnement,
CEA/CNRS, Gif-sur-Yvette, France

Abstract

In this chapter we examine how aerosol and cloud fields undergo perturbations by anthropogenic activities. Recent surface observations and satellite remote sensing have detected signatures of large-scale changes in the atmospheric aerosol amounts, associated changes in the cloud fraction, and microphysical structures on a global scale. Models can simulate these signatures fairly well, but problems still remain. Fields of anthropogenic aerosol optical depth (AOD) from several atmospheric models have been found to be consistent with the spatial pattern obtained from satellite data. Further studies are needed to differentiate between natural and anthropogenic aerosols and to interpret observed temporal and regional trends in aerosol parameters. The strength of the cloud–aerosol interaction can be characterized by the regression of AOD or aerosol index (AI) on cloud droplet number (N_c). From recent studies, the corresponding slopes $d\log(N_c)/d\log(A)$ vary between 0.19 and 0.7. Further work is needed to see whether such variability is the result of methodological problems or differences in cloud environments for which the studies have established the cloud–aerosol relation.

Introduction

Our understanding and, hence, modeling of the aerosol and cloud system is mired by large uncertainties. As we attempt to characterize the extent to which clouds are perturbed by humankind in modern times, we cannot afford to

Chapter from:
Clouds in the Perturbed Climate System, edited by Jost Heintzenberg and Robert J. Charlson.
2009. Strüngmann Forum Report, vol. 2. Cambridge, MA: MIT Press. ISBN 978-0-262-01287-4

ignore any process, even those that are still unknown. It is imperative for us to accumulate evidence of the changing atmospheric particle environments.

In this chapter, we present the signature and features of changing aerosols, clouds, and radiation fields, because these provide evidence of alterations in the clouds and radiation budget by aerosols on the global scale. Thereafter we discuss changes attributable to natural and anthropogenic causes, as quantified by satellite remote sensing and surface measurements, which have greatly improved over the last two decades.

We begin by reviewing studies that report on the anthropogenic perturbation of the aerosol system, which may, in turn, perturb clouds. At the present time, our understanding of aerosol–cloud interactions is not acute enough to extrapolate an aerosol perturbation into measurable cloud characteristics. Based on the evidence of the perturbations in the aerosol system, we propose a framework for studies that have quantified the relationship between aerosol parameters and cloud properties (e.g., cloud optical thickness, cloud droplet radius, or liquid water path) to be subsequently reviewed. Other Earth system components (e.g., greenhouse gas levels or altered land surface attributable to land use), though important, are not addressed, as these fall outside the focus of our mandate. We wish to emphasize, however, that they cannot be ignored, as they may also contribute to the perturbation of the cloud system.

Large-scale Changes of Aerosols

Anthropogenic trace substances can be currently found in precipitation everywhere around the globe as a result of the long-range transport of aerosols. In a strict sense, it is impossible nowadays to study a pristine natural atmosphere. However, if we are to identify or quantify the degree of anthropogenic perturbation, we must have an understanding of pristine conditions. Several methods have been used to estimate and characterize the anthropogenic fraction of aerosols:

- chemical analysis of ice core data,
- analysis of observed recent trends of aerosol parameters,
- characterization of differences in clean and polluted areas of aerosol composition,
- process understanding of natural aerosol emissions,
- reconstruction of the evolution of anthropogenic emissions,
- transport modeling of preindustrial and present-day conditions.

Ultimately, characterization needs to translate the uncertainty of anthropogenic aerosol perturbation into the uncertainty of any particular process involving aerosols and inducing a cloud perturbation. Some findings that indicate an anthropogenic perturbation of atmospheric aerosols may not be directly relevant to the cloud system (e.g., sulfate deposition on the high plateau of

Chapter from:
Clouds in the Perturbed Climate System, edited by Jost Heintzenberg and Robert J. Charlson.
2009. Strüngmann Forum Report, vol. 2. Cambridge, MA: MIT Press. ISBN 978-0-262-01287-4

Greenland). However, they may still provide an estimate of the extent of the aerosol perturbation, which could ultimately be related to parameters directly relevant for the cloud system.

In this section we address the following questions:

- What is the history of anthropogenic perturbations to the aerosol content of the atmosphere, and how does it compare to present-day conditions? Is a historical versus current view of perturbations consistent with our knowledge of anthropogenic emissions?
- What is the current regional distribution of anthropogenic aerosols?
- How can we translate anthropogenic perturbations of aerosol parameters (e.g., deposition, mass concentration, optical depth and emissions) into perturbations of parameters relevant for clouds (e.g., cloud condensation nuclei (CCN) concentrations and radiative budgets)?

Anthropogenic Perturbation of the Aerosol Content in the Atmosphere

Glaciers provide an invaluable record of past precipitation. Deep ice cores reveal information on the preindustrial concentration levels of key aerosol components. However, the anthropogenic enhancement of these concentrations visible in the most recent snow deposits, compared to the preindustrial levels, can only be regarded as minimal estimates of aerosol perturbation levels in the atmosphere, as most glaciers are located far from primary anthropogenic source regions. Thus, such estimates can only reflect a diluted state of the perturbed atmosphere. Actual levels for specific regions or for a global average will most likely be higher.

Sulfate concentrations in ice cores suggest that aerosol concentrations increased dramatically as of 1900 and continued at an elevated level until ca. 1950, after which they rose steeply until 1980. As of 1980, levels began to decline, coincident with the introduction of sulfur dioxide abatement schemes in power plants. In 1980, an approximate fourfold increase in sulfate concentrations, compared to preindustrial levels, was found in Greenland and the Canadian Arctic (Legrand et al. 1997; Goto-Azuma and Koerner 2001). In the Alps, ice cores show larger increases, attributable to their proximity to European industrial sources. In the Alps, Preunkert et al. (2001) observed that sulfate concentrations in ice increased from preindustrial levels of 80 ng g^{-1} to 860 ng g^{-1} in 1980, followed by a decrease to 600 ng g^{-1} in the 1990s; that is, sulfate was enhanced anthropogenically by a factor of ten. Goto-Azuma and Koerner (2001) found that nitrate levels in the Arctic stayed at preindustrial levels until 1950, after which it began to climb up until the 1980s, reflecting an anthropogenic enhancement by a factor of 2–3. Black carbon trends in Greenland seem to demonstrate that a maximum level (a fivefold increase over the levels from 1870) was reached by 1920. Air pollution control measures reduced these levels by 1950 (McConnell et al. 2007), decoupling the black

Chapter from:
Clouds in the Perturbed Climate System, edited by Jost Heintzenberg and Robert J. Charlson.
2009. Strüngmann Forum Report, vol. 2. Cambridge, MA: MIT Press. ISBN 978-0-262-01287-4

carbon trend in Greenland from that of sulfate after 1940. Compared to the early 19th century, it appears that current black carbon concentrations were enhanced only by a factor of two (McConnell et al. 2007). The correlation analysis by McConnell et al. suggests that fires from conifer-rich boreal forests were, and still are, responsible for these levels at this site. Several other studies support the general trends of sulfate, nitrate, and black carbon in ice cores, either through a direct comparison to emission scenarios or through transport modeling studies (e.g., Boucher and Pham 2002; Preunkert et al. 2001).

Trends established for the last decades indicate that the modern-day perturbation of anthropogenic aerosols is changing. From AVHRR retrievals, Mishchenko et al. (2007b) derived a global decrease (only over the ocean) of total AOD, from 0.14 (1988–1990) to 0.11 (2003–2005). If this trend was caused solely by anthropogenic aerosol changes, then this would represent a relatively large increase as compared to model estimates for the year 2000: oceanic anthropogenic AOD of 0.022 (Schulz et al. 2006). If both models and observations are correct, then by the end of the 1980s, anthropogenic AOD should have been as high as 0.05, exerting a direct aerosol forcing effect two times greater than today. However, total global aerosol emissions have not been reported to have decreased by a factor of two since 1980. Natural aerosol trends and climate-driven changes in columnar aerosol burdens may have influenced these AOD trends, but it is questionable whether we understand past emission trends well enough, or whether we have misjudged the capability of the satellite sensors to detect trends or the models to derive an anthropogenic AOD. It is worth noting that a recent decrease in tropospheric AOD may have contributed to the modern-day increases in measurements for surface solar fluxes. Several sites of the BSRN network show increases after 1990 in downward solar radiation of 5–10 W m^{-2}, whereas a decline of the same order of magnitude in surface solar fluxes was observed between 1960 and 1990 (Wild et al. 2005; Liepert and Tegen 2002).

Since around 1970, systematic measurements of *in-situ* aerosol properties have been performed at surface sites (e.g., aerosol extinction, absorption, aerosol composition, concentration and wet deposition), and several authors have attempted to analyze the trends. For the Arctic, Quinn et al. (2007) report that in Alert, Alaska, from 1982–2004, peak concentrations of particulate sulfate decreased from 0.8–0.3 μg S m^{-3}. Peak black carbon levels at Alert decreased only slightly, from 250 ng m^{-3} in 1990 to 150 ng m^{-3} in 2000, whereas absorption measurements in Barrow showed almost no trend during 1990–2005. Scattering is reported to have decreased from 20 mm^{-1} in 1980 to a minimum of 10 mm^{-1} in 1995, and since then it is reported to be increasing again. Based on a model analysis of observed concentrations, Heidam et al. (2004) reports that particulate sulfate has decreased by 30% in Northern Greenland between 1990 and 2000.

Such trends are sometimes related to regional changes in emissions. A recent example is the increase in East Asian emissions, which has most prominently

Chapter from:
Clouds in the Perturbed Climate System, edited by Jost Heintzenberg and Robert J. Charlson.
2009. Strüngmann Forum Report, vol. 2. Cambridge, MA: MIT Press. ISBN 978-0-262-01287-4

been detected by satellites to reveal increases in NO_2 (Richter et al. 2005) and AOD (Mishchenko et al. 2007a). Modern regional aerosol trends are potentially important, because they allow cloud–aerosol interactions to be tested using modern instrumentation.

Regional Distribution of Anthropogenic Aerosols and Forcing Efficiency

Two arguments support the idea that a better understanding of anthropogenic AOD would help our understanding of perturbed clouds. First, global coverage of satellite-derived AOD and its interpretation in terms of natural or anthropogenic origin are crucial if we are to understand regional differences, for example, in cloud perturbation. Second, a considerable number of studies use AOD–cloud–parameter relationships to understand aerosol-induced cloud perturbations; thus, the anthropogenic contribution to total AOD is of primary interest. Ice core data and long-term, intensive *in-situ* observations are sparse, yet they need to be assimilated to derive a large-scale assessment of the anthropogenic perturbation by large-scale models, surface networks, or remote sensing. In other words, different types of information need to be integrated if we are to derive global anthropogenic AOD fields.

Spaceborne sensors cannot easily distinguish between anthropogenic and natural aerosols. However, retrievals based on multi-wavelength sensors, such as the MODIS instrument, make use of the dependence of light scattering on particle size. Since most anthropogenic aerosol particles of relevance are caused by combustion processes, they often dominate the fine-mode fraction of the aerosol particles. A fine-mode AOD fraction can be estimated from the wavelength-dependent aerosol extinction signal. From this notably dimethylsulfide-derived sulfate, fine fractions of dust and sea salt as well as natural biomass burning must be subtracted before the fine-mode AOD signal can be interpreted as anthropogenic. Kaufman et al. (2005) suggest classifying the MODIS observations according to dominant aerosol types. In doing so, the average fractions of additional aerosols can be estimated and global maps of anthropogenic AOD constructed. These global maps can be compared to model estimates of the anthropogenic AOD, which are based on the difference of a simulation of preindustrial and present-day conditions. To demonstrate, we compare in Figure 17.1 the MODIS-derived anthropogenic AOD field and the corresponding modeled field for the month of July, using LMDzT–INCA (see description in Kinne et al. 2006 and Textor et al. 2006). The general patterns of high anthropogenic AOD values close to the industrialized coasts as well as to South Africa show up in both the satellite data analysis and model simulation.

A broader comparison is desirable to document our understanding of anthropogenic AOD. In addition, model data should be filtered for the presence of MODIS observations to obtain comparable global averages. This can be done by using the AeroCom project aerosol model intercomparison results, as described by Schulz et al. (2006), and six years of MODIS observations. In

Chapter from:
Clouds in the Perturbed Climate System, edited by Jost Heintzenberg and Robert J. Charlson.
2009. Strüngmann Forum Report, vol. 2. Cambridge, MA: MIT Press. ISBN 978-0-262-01287-4

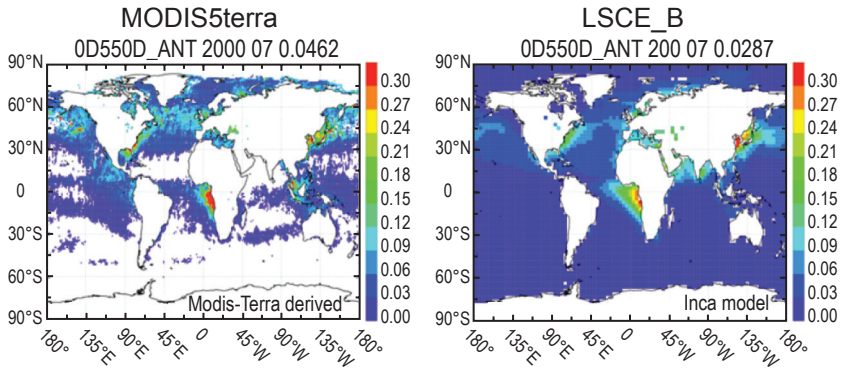

Figure 17.1 Anthropogenic aerosol optical depth as derived from MODIS fine-mode AOD and total AOD using the calculation proposed by Kaufman et al. 2005 (left figure) for the month of July, 2000. INCA anthropogenic AOD is derived from two simulations using AeroCom present-day and preindustrial emissions.

Figure 17.2, a range of multiannual observations with MODIS is established for each month and shown together with the individual model-derived seasonal cycles. The figure indicates considerable interannual variability in the MODIS-derived anthropogenic AOD. A maximum is observable in early summer, and values seem to be slightly higher in late autumn than in winter and early spring. However, the observed seasonal cycle is small, yet seasonal amplitude is the same size as the interannual variability itself. Model-derived anthropogenic AOD is, on average, below the MODIS-derived values. Since all models used

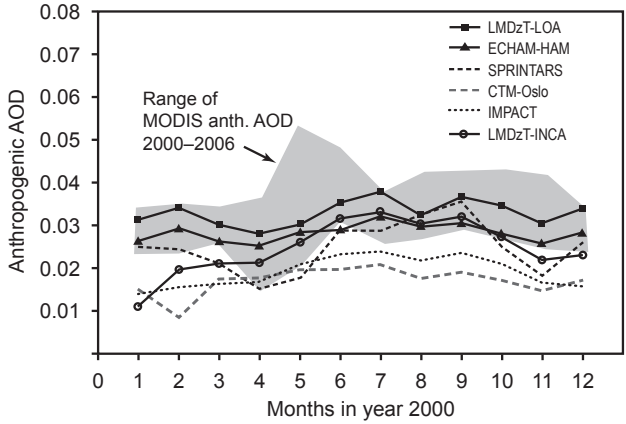

Figure 17.2 Ocean-only anthropogenic aerosol optical depth simulated by AeroCom models and derived from a MODIS collection of five fine-mode and total AOD (after Kaufman et al. 2005). The light gray band shows the data range from six years of MODIS data. Model-simulated AOD fields are filtered for presence of MODIS 2001 observations. The models used meteorological fields for the year 2000 and AeroCom emissions from year 2000 and 1750.

Chapter from:
Clouds in the Perturbed Climate System, edited by Jost Heintzenberg and Robert J. Charlson.
2009. Strüngmann Forum Report, vol. 2. Cambridge, MA: MIT Press. ISBN 978-0-262-01287-4

the same seasonal cycle of emissions, a particular observation can be made to explain consistently low values in April/May and higher values in late boreal summer. Note, however, that the monthly AOD evolution is not highly correlated among models. If we assume that the general transport conditions were rather similar if not identical, because reanalyzed meteorological fields from the year 2000 were used in all models, then we would find variance in the lifetime of anthropogenic aerosols and, hence, removal processes between models.

Altogether, we can conclude that two independent methods show rather similar results with respect to an estimate of the anthropogenic AOD. Satellite-derived estimates of the anthropogenic AOD are slightly higher. Interannual variability, as derived from six years of MODIS observations and intermodel diversity, are of similar magnitude. The monthly anthropogenic AOD, as derived from the two methods, is found in a band ranging from 0.01 to 0.05, which may be interpreted as an estimate of the uncertainty range of this parameter. Table 17.1 summarizes differences in AOD between land and ocean. Both satellite-derived estimates and model results suggest that anthropogenic AOD over land is on a global average three times higher than over ocean.

In addition to regional differences in anthropogenic AOD, the sensitivity of the radiative balance or the cloud system to AOD may also vary regionally. It would thus be useful to study this sensitivity in greater detail. As a first step, we investigate a forcing efficiency, which is defined as the ratio of total direct aerosol radiative forcing (RF) over anthropogenic AOD. By looking at forcing efficiencies, one may characterize the way aerosols influence directly the radiative balance of the Earth. One must eliminate variation of the RF attributable to

Table 17.1 AeroCom model simulation results of anthropogenic aerosol optical depth (AOD), top-of-the-atmosphere radiative forcing (RF), and forcing efficiency per unit optical depth (NRF). Grid-box area-weighted means are given over land and ocean in clear-sky conditions between 60°S and 60°N. Observation-based values reported by Yu et al. (2006).

Model	Ocean			Land		
	AOD	RF ($W\ m^{-2}$)	NRF ($W\ m^{-2}\ \tau^{-1}$)	AOD	RF ($W\ m^{-2}$)	NRF ($W\ m^{-2}\ \tau^{-1}$)
UMI	0.019	–0.68	–38	0.057	–1.33	–24
UIO_CTM	0.018	–0.69	–45	0.058	–1.64	–28
LOA	0.033	–0.67	–16	0.093	–1.47	–14
LSCE	0.025	–0.89	–34	0.064	–1.35	–21
MPI.HAM	0.023	–0.57	–26	0.075	–1.10	–24
GISS	0.011	–0.33	–38	0.026	–0.42	–17
SPRINTARS	0.026	–0.32	–11	0.081	–0.63	–14
AeroCom mean	0.022	–0.59	–29	0.065	–1.14	–20
Yu et al. (2006)	0.031	–1.10	–37	0.088	–1.80	–20

Chapter from:
Clouds in the Perturbed Climate System, edited by Jost Heintzenberg and Robert J. Charlson.
2009. Strüngmann Forum Report, vol. 2. Cambridge, MA: MIT Press. ISBN 978-0-262-01287-4

simple variation of AOD. A spatial variation in forcing efficiency indicates that aerosols in various regions perturb the radiative budget differently. Table 17.1 reports how the clear-sky forcing efficiency may differ between land and ocean regions (Schulz et al. 2006; Yu et al. 2006). It appears that the forcing efficiency is almost twice as negative over the ocean. Several factors influence the forcing efficiency: particle absorption and hemispheric backscatter, surface albedo, vertical distribution of aerosols and of the atmospheric temperature. The more negative forcing efficiency values, observed over the ocean, are attributable to higher land than ocean surface albedo and more absorbing anthropogenic aerosols over land. The comparison to the observationally based estimate reveals that both the anthropogenic AOD and the clear-sky forcing efficiency are smaller in the models. Thus, both factors contribute to a smaller direct aerosol forcing value derived from the AeroCom models.

Finally, we suggest that there are only very few regions in which the direct radiative effect of aerosols is considerably perturbed by anthropogenic aerosols. The compilation of modeled forcing fields by Schulz et al. (2006) can be used to see where the major contributions to the total direct aerosol forcing can be expected. This may guide efforts to improve our understanding of the aerosol forcing through measurements. Table 17.2 reports the area fraction in which significantly negative clear-sky forcing with values less than –2 Wm^{-2} can be found in the models. The contribution of the forcing from that area to the total direct aerosol forcing is then computed for each model. As a result, 45–65% of the clear-sky direct aerosol forcing is expected to originate from only 10–15% of the Earth's surface.

Anthropogenic CCN Enhancements and Aerosol Forcing

Anthropogenic perturbations of the various aerosol parameters can impact the cloud system through different processes. Of direct relevance is that part of the aerosol particle spectrum which can act as CCN. In addition, any change in the

Table 17.2 Global area fraction *A* in which clear-sky direct aerosol forcing (CS–RF) is more negative than –2 W m^{-2} in six AeroCom models and contribution of clear-sky direct aerosol forcing in this area to total clear-sky forcing by aerosols.

	Area fraction *A*, where CS–RF < –2 Wm^{-2}	Area fraction *A*, where CS–RF < –2 Wm^{-2}
LOA	14%	64%
LSCE	14%	54%
UMI	10%	44%
UIO-CTM	11%	60%
MPI-HAM	13%	59%
SPRINTARS	9%	55%

Chapter from:
Clouds in the Perturbed Climate System, edited by Jost Heintzenberg and Robert J. Charlson.
2009. Strüngmann Forum Report, vol. 2. Cambridge, MA: MIT Press. ISBN 978-0-262-01287-4

temperature profile within the troposphere resulting from direct RF will perturb cloud formation. For both CCN concentrations and RF, similar problems are encountered as we attempt to investigate their anthropogenic perturbation and role in the perturbation of clouds:

- No direct observations exist in the preindustrial or pristine atmosphere.
- Current observations are difficult and sparse, or have just recently been initiated.
- Anthropogenic and natural components cannot strictly be observed independently in the ambient atmosphere.
- The relationship between observable parameters (e.g., particle concentration, composition, size distribution, optical depth, phase function and CCN concentration) and the direct/indirect radiative effect of the aerosol depends on the meteorological and chemical environment.
- Both natural and anthropogenic components need to be known to assess properly the potential of CCN and RF to perturb clouds.

Deriving or estimating pristine CCN concentrations requires a conceptual model or a full aerosol–chemistry model, verified with caution against remote, clean locations of the globe. Recently, Andreae (2007) suggested that continental and oceanic CCN concentrations may have been similar, which would contrast current conditions, where polluted regions show typical enhancements of 50–300% over remote regions. A better understanding of the anthropogenic CCN concentrations is needed and, when available, will most likely have considerable impact on the modeling of the aerosol indirect effect. It is worth noting that the majority of climate models assume a rather simple relationship of anthropogenic sulfate aerosol mass and cloud properties (Boucher and Lohmann 1995); they neglect any variation in natural aerosols or other aerosol components that would indirectly alter the relationship between sulfate mass and CCN.

A slightly more straightforward assessment can be made for direct RF by aerosols. Multicomponent aerosol models are positioned to become state-of-the-art tools for the estimation of global aerosol RF. Within AeroCom, nine different global models with detailed aerosol modules have independently produced instantaneous direct RF as a result of anthropogenic aerosols (Schulz et al. 2006). Figure 17.3 shows the major components needed to characterize direct and semi-direct aerosol forcing as maps, illustrating the spatial location of such direct aerosol forcing. For the semi-direct effect, Figure 17.3d displays the solar atmospheric forcing (the difference between top of the atmosphere and surface forcing), which heats the atmospheric column and has thus the potential to influence the formation of clouds. This forcing is estimated at +0.82 ± 0.17 W m^{-2}. The local annual average maxima of this atmospheric forcing exceed +5 W m^{-2}, confirming the regional character of aerosol impacts on climate. Such regional warming of the atmospheric column attributable to

Chapter from:
Clouds in the Perturbed Climate System, edited by Jost Heintzenberg and Robert J. Charlson.
2009. Strüngmann Forum Report, vol. 2. Cambridge, MA: MIT Press. ISBN 978-0-262-01287-4

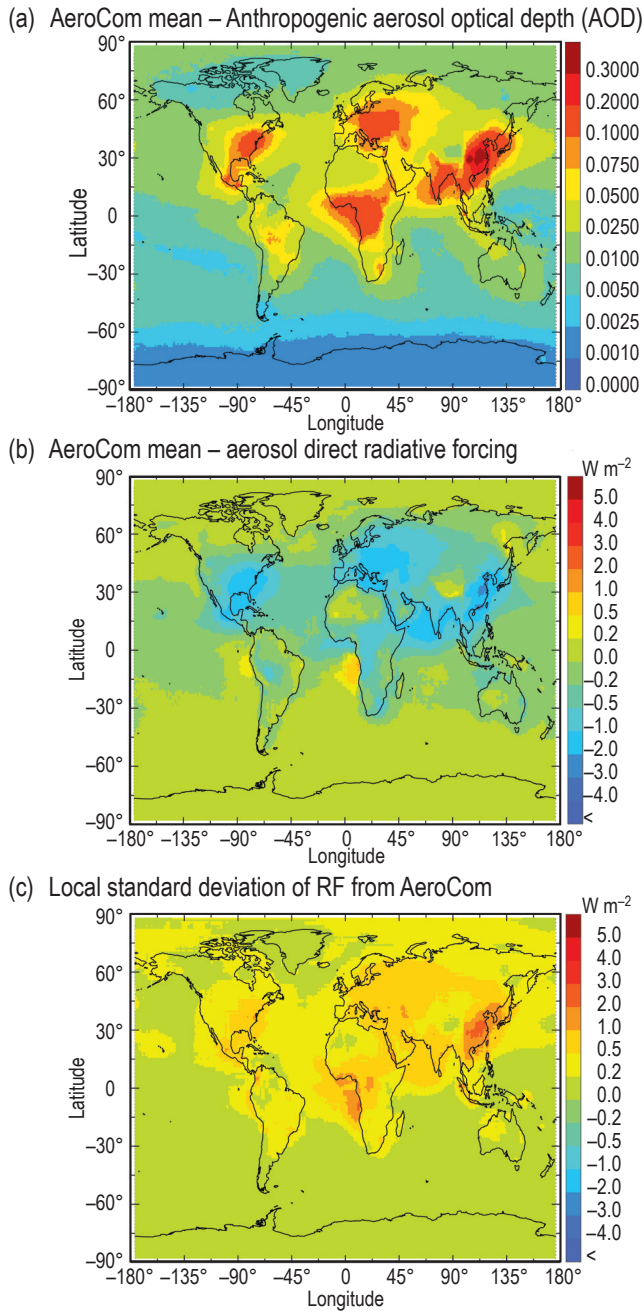

Figure 17.3 Mean annual fields derived from the regridded AeroCom model simulations of (a) anthropogenic aerosol optical depth; (b) total direct aerosol radiative forcing; (c) local standard deviation of radiative forcing (RF) from nine models.

Chapter from:
Clouds in the Perturbed Climate System, edited by Jost Heintzenberg and Robert J. Charlson.
2009. Strüngmann Forum Report, vol. 2. Cambridge, MA: MIT Press. ISBN 978-0-262-01287-4

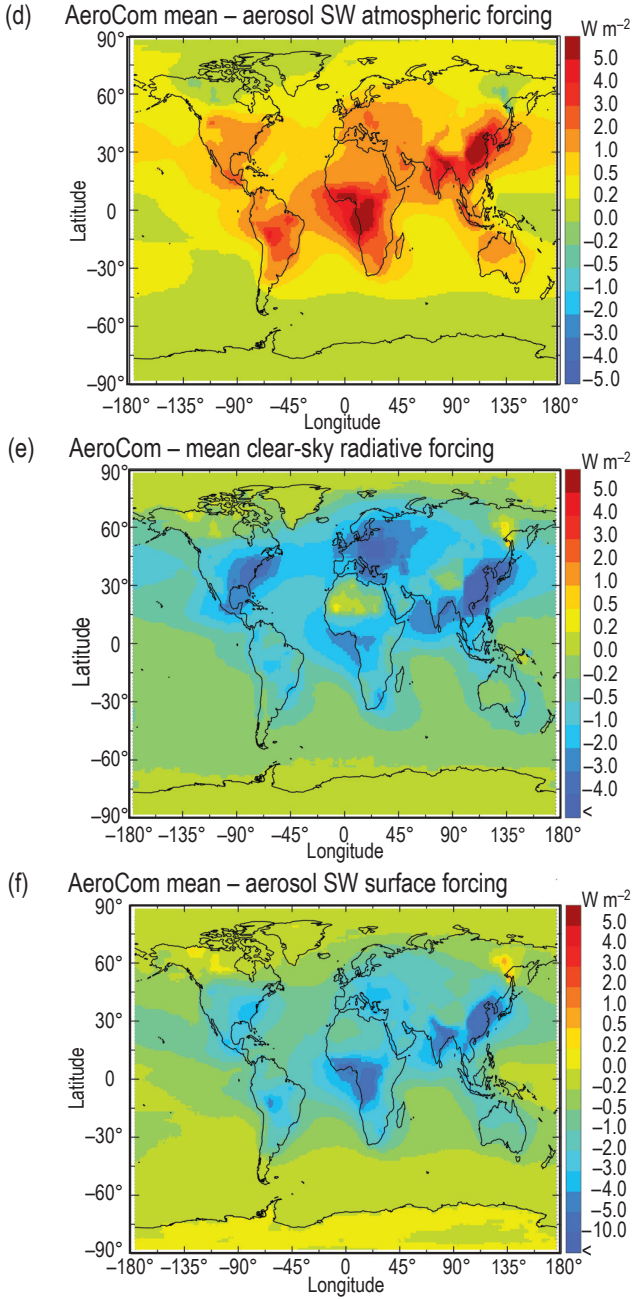

Figure 17.3 (continued) (d) Atmospheric shortwave forcing of column by aerosols; (e) clear-sky aerosol RF; (f) aerosol surface forcing. See values in Table 5 of Schulz et al. (2006).

Chapter from:
Clouds in the Perturbed Climate System, edited by Jost Heintzenberg and Robert J. Charlson.
2009. Strüngmann Forum Report, vol. 2. Cambridge, MA: MIT Press. ISBN 978-0-262-01287-4

solar absorption by soot has been measured, for example, in the outflow of the Indian subcontinent (Ramanathan et al. 2007). In terms of the amplitude of the hydrological cycle, the annual average surface forcing is estimated to be $-1.02 \pm 0.23 \mathrm{Wm}^{-2}$.

In Working Group I's contribution to the IPCC Fourth Assessment Report, Forster et al. (2007) summarized current knowledge on global estimates of the direct RF at the top of the atmosphere:

> A central model-derived estimate for the aerosol direct RF is based here on a compilation of recent simulation results using multi-component global aerosol models...This is a robust method for several reasons. The complexity of multi-component aerosol simulations captures nonlinear effects. Combining model results removes part of the errors in individual model formulations. As shown by Textor et al. (2006), the model-specific treatment of transport and removal processes is partly responsible for the correlated dispersion of the different aerosol components. A less dispersive model with smaller burdens necessarily has fewer scattering and absorbing aerosols interacting with the radiation field. An error in accounting for cloud cover would affect the all-sky RF from all aerosol components. Such errors result in correlated RF efficiencies for major aerosol components within a given model. Directly combining total aerosol RF results gives a more realistic aerosol RF uncertainty estimate. The AeroCom compilation suggests significant differences in the modeled local and regional composition of the aerosol…, but an overall reproduction of the total [AOD] variability can be performed (Kinne et al. 2006). The scatter in model performance suggests that currently no preference or weighting of individual model results can be used (Kinne et al. 2006). The aerosol RF taken together from several models is more robust than an analysis per component or by just one model. The mean estimate…of the total aerosol direct RF is -0.2 W m^{-2}, with a standard deviation of ± 0.2 W m^{-2}. This is a low-end estimate for both the aerosol RF and uncertainty because nitrate (estimated as -0.1 W m^{-2}…) and anthropogenic mineral dust (estimated as -0.1 W m^{-2}…) are missing in most of the model simulations. Adding their contribution yields an overall model-derived aerosol direct RF of -0.4 W m^{-2} (90% confidence interval derived from 20 model results: 0 to -0.8 W m^{-2}).
>
> Three satellite-based measurement estimates of the aerosol direct RF have become available, which all suggest a more negative aerosol RF than the model studies…Bellouin et al. (2005) computed a TOA aerosol RF of -0.8 ± 0.1 W m^{-2}. Chung et al. (2005), based upon similarly extensive calculations, estimated the value to be -0.35 ± 0.25 W m^{-2}, and Yu et al. (2006) estimated it to be -0.5 ± 0.33 W m^{-2}. A central measurement-based estimate would suggest an aerosol direct RF of -0.55 W m^{-2}. Figure 2.13 [of the IPCC report] shows the observationally based aerosol direct RF estimates together with the model estimates published since the TAR [Third Assessment Report] and the AeroCom model results.

Note that the measurement-based estimate is based on very few estimates and should be understood as the result of an expert assessment rather than the result of a statistic analysis:

Chapter from:
Clouds in the Perturbed Climate System, edited by Jost Heintzenberg and Robert J. Charlson.
2009. Strüngmann Forum Report, vol. 2. Cambridge, MA: MIT Press. ISBN 978-0-262-01287-4

> The discrepancy between measurements and models is also apparent in oceanic clear-sky conditions where the measurement-based estimate of the combined aerosol direct radiative effect (DRE) including natural aerosols is considered unbiased. In these areas, models underestimate the negative aerosol DRE by 20 to 40% (Yu et al. 2006). The anthropogenic fraction of [AOD] is similar between model and measurement based studies. Kaufman et al. (2005) used satellite-observed fine-mode [AOD] to estimate the anthropogenic [AOD]. Correcting for fine-mode [AOD] contributions from dust and sea salt, they found 21% of the total [AOD] to be anthropogenic, while the [model compilation] suggests that 29% of [AOD] is anthropogenic. Finally, cloud contamination of satellite products, aerosol absorption above clouds, not accounted for in some of the measurement-based estimates, and the complex assumptions about aerosol properties in both methods can contribute to the present discrepancy and increase uncertainty in aerosol RF. (Forster et al. 2007, p. 169, 171)

Considering that the observational and model-based forcing estimates represent both valid methods, the IPCC assessed that an intermediate direct aerosol RF estimate with a large uncertainty (–0.5 [–0.9 to –0.1] W m^{-2}) reflects our current knowledge, containing most available RF estimates. The forcing chart expresses satisfactorily the important role that aerosols play as the major greenhouse gas opponent in constituting the total anthropogenic forcing of current climate (for further discussion, see Haywood and Schulz 2007).

Cloud Field Change and Aerosol Effects

Evidence of perturbed clouds on the global scale are more difficult to pinpoint from observations because spatial and temporal variations of the cloud field are large and complex. The effective droplet radius (CDR) of water clouds has been used frequently to study the signature of perturbed clouds because the spatial distribution of CDR is relatively homogeneous, even when clouds show a large variability in the cloud optical thickness (COT). Large-scale signatures, such as enhanced COT of ship trail clouds, and reduced CDR around the continents have been observed from satellites (Coakley et al. 1987; Radke et al. 1989; Nakajima et al. 1991; Han et al. 1994; Kawamoto et al. 2001). Kawamoto and Nakajima (2003) reported distinct seasonal changes of CDR, depending on location. However, an observed long-term change of CDR could not be clearly linked to either an interannual change in cloud perturbation or a shift in the satellite's orbit. These signatures can be compared with the sulfate emission increase in the populated regions to establish a link between human activity and satellite-derived regional signatures (Chameides et al. 2002; Kawamoto et al. 2004, 2006). Comparison of satellite-observed aerosol and cloud parameters is a more direct approach to investigate the mechanism of the phenomena. This approach has become more useful since satellite-derived aerosol and cloud products were constructed from various satellite imagers: AVHRR, POLDER,

Chapter from:
Clouds in the Perturbed Climate System, edited by Jost Heintzenberg and Robert J. Charlson.
2009. Strüngmann Forum Report, vol. 2. Cambridge, MA: MIT Press. ISBN 978-0-262-01287-4

MODIS, and GLI (King et al. 1999). We note that detailed interpretation using models is indispensable. The preceding discussion shows that the global distribution of total AOD at a wavelength of 550 nm (AOD) can be observed and modeled within an accuracy of 0.05.

Figure 17.4 shows global distributions of the CDR in water clouds derived from a MODIS and MIROC+SPRINTARS global climate simulation (Takemura et al. 2006). Here the area of large aerosol loading corresponds well to the area of reduced CDR, with values as small as 8 μm, both in the satellite and model results. The observed aerosol plumes are much larger in the North Pacific and smaller in the northern Indian Ocean than simulated

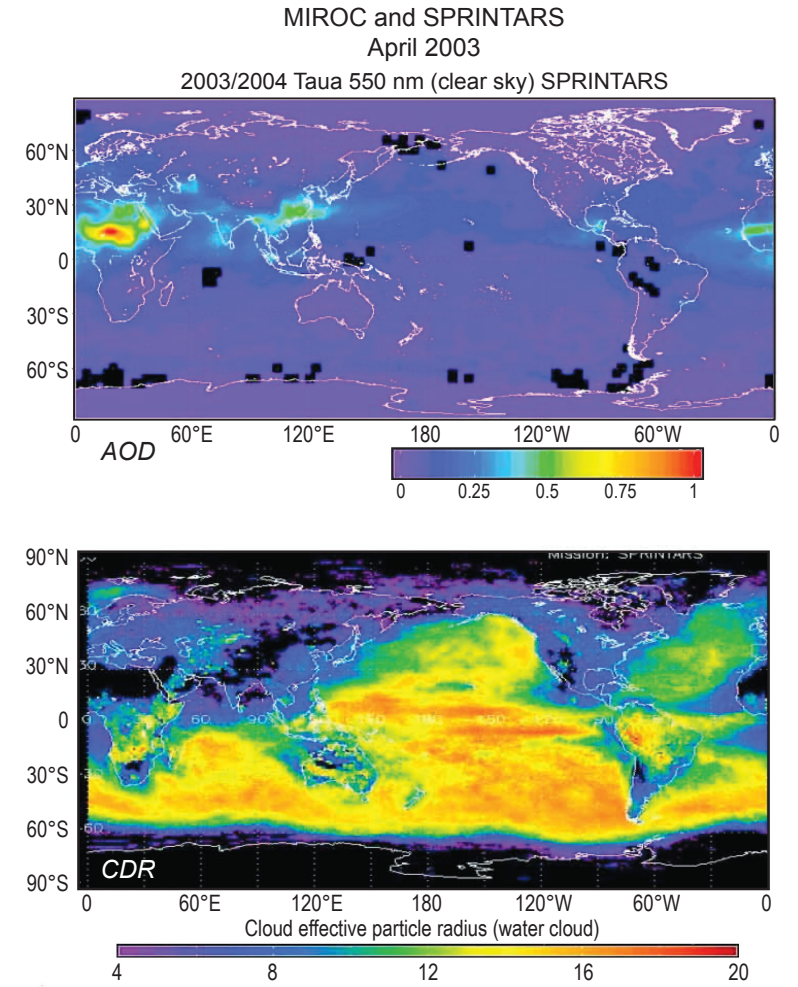

Figure 17.4 Satellite (MODIS)-observed and model (MIROC+SPRINTARS)-simulated global distributions of AOD and CDR for water clouds.

Chapter from:
Clouds in the Perturbed Climate System, edited by Jost Heintzenberg and Robert J. Charlson.
2009. Strüngmann Forum Report, vol. 2. Cambridge, MA: MIT Press. ISBN 978-0-262-01287-4

ones. It is interesting to note that a corresponding similarity is also found in the observed and simulated CDR fields; that is, the elongated area of small CDR is much wider in observations than in simulation in the North Pacific and vice versa in the Indian Ocean. This indicates that the northern Pacific aerosol plume in the satellite result seems to be real and responsible for the reduced CDR in this area, even though the aerosol remote sensing is known to overestimate coarse-mode particles attributable to cloud contamination. Clearly, this example shows that a careful analysis is needed to extract the real signature of aerosol–cloud interactions, as both models and satellite systems have their own problems.

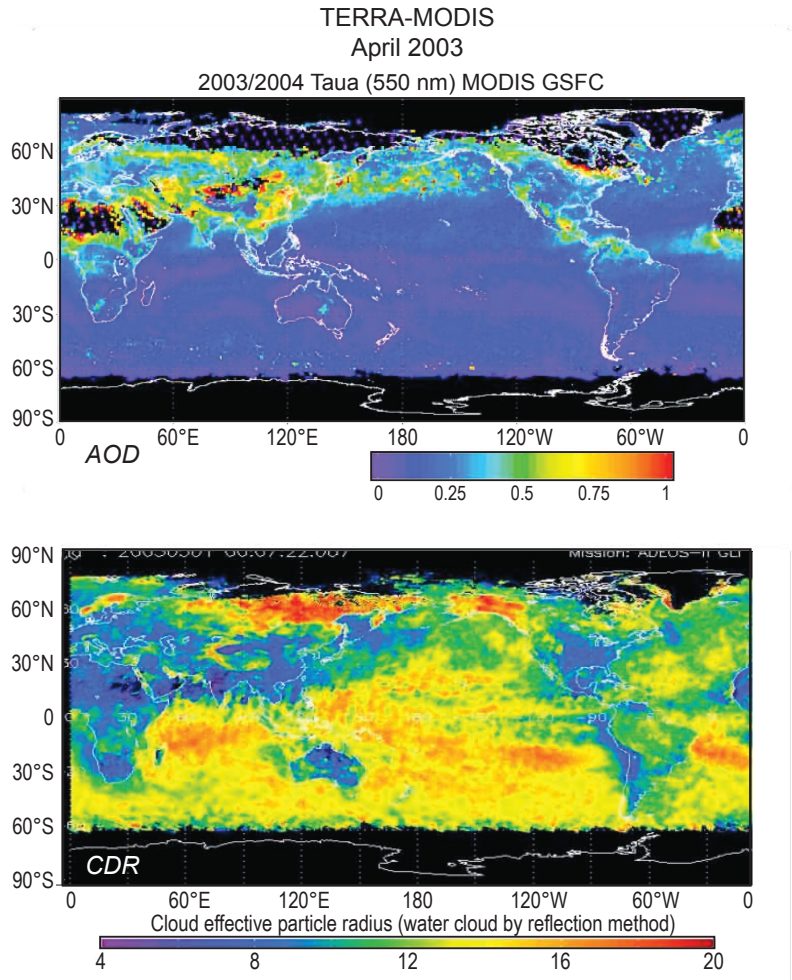

Figure 17.4 (continued) Monthly mean of April 2003 (provided by NASA MODIS team, Takashi Y. Nakajima and Toshihiko Takemura).

Chapter from:
Clouds in the Perturbed Climate System, edited by Jost Heintzenberg and Robert J. Charlson.
2009. Strüngmann Forum Report, vol. 2. Cambridge, MA: MIT Press. ISBN 978-0-262-01287-4

Change in the Cloud Microphysical Condition

The strength of aerosol–cloud interactions can be evaluated by the following regression between satellite-observed cloud parameter for water clouds (Y) and columnar particle concentrations (A):

$$Y = a(Y) + b(Y) \log (A), \tag{17.1}$$

where *log* stands for the base 10 logarithm (log_{10}), and $a(Y)$ and $b(Y)$ are regression coefficients to be determined from the analysis. McComiskey and Feingold (2008) discussed that the slopes of various cloud parameters are interrelated for linearly stratified clouds and are useful to evaluate the first indirect forcing of aerosols, which is the cloud forcing when aerosols act as CCN under the condition of a fixed cloud liquid water path (LWP). Many past studies use AOD as a proxy for the aerosol columnar particle concentrations, A.

Some studies use AOD for fine-mode aerosols (AOD-fine) of the NASA's MODIS product as a better index for A. Others use the aerosol index, AI=$\alpha \times AOD$, calculated from satellite-derived AOD and Ångström exponent (α), which is an invariant without large dependence on the size distribution of optically relevant particles (Nakajima et al. 2001; Bréon et al. 2002). This AI correlates fairly well with the column aerosol particle number (N_a) in the optically important particle radius range larger than about 0.05 μm. Some studies directly use N_a, calculated from satellite aerosol observables and an assumed size distribution, the latter being the most relevant parameter for the cloud nucleation process. We should bear in mind, however, that A = AOD may cause artifacts as a result of increasing particle size through adsorbed water vapor at high relative humidities (e.g., the magnitude of slope b might be underestimated when A = AOD.) Other artifacts, as discussed later for each cloud parameter, arise from using a simple regression analysis, as in Equation 17.1, to elucidate the causes and results of the interaction. Here, it is not possible to address all of these differences; however, we believe that it is useful to summarize past results to see the differences and commonalities between them. Future studies should investigate detailed variances of sampling conditions, target clouds, and models to eliminate artifacts, which may exist in our simple comparison.

One consideration, in terms of cloud physics, suggests that a relation between N_a and cloud droplet number (N_c) can be approximated by a form, as in Equation 17.1, with $Y = \log(N_c)$. Table 17.3 and Figures 17.5–17.7 summarize past reported values of the corresponding slope $b(\log N_c) = d\log(N_c)/d\log(A)$ from Equation 17.1, with A = AOD, AI, or N_a (as indicated in the third column of Table 17.3); other frequently used slopes are explained later. In Table 17.3, values for different aerosol concentration indices (AOD, AI, and N_a) are roughly compared without correction, under the assumption that the regression slope does not change when a linear proportionality among them is assumed. Figure 17.5 indicates that $b(\log N_c)$ ranges widely from 0.19–0.7, which is

Chapter from:
Clouds in the Perturbed Climate System, edited by Jost Heintzenberg and Robert J. Charlson.
2009. Strüngmann Forum Report, vol. 2. Cambridge, MA: MIT Press. ISBN 978-0-262-01287-4

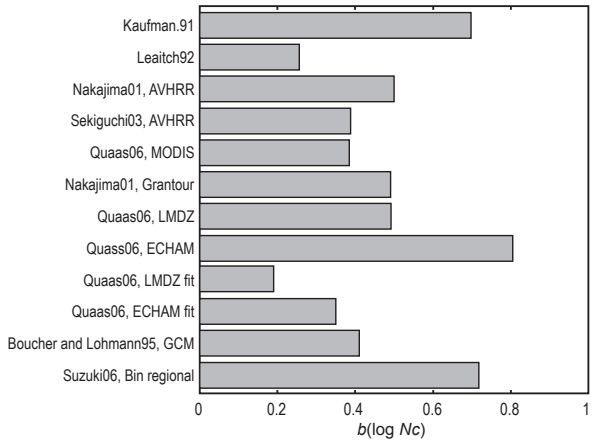

Figure 17.5 Reported values of the regression slope $b(\log N_c)$ (see Table 17.3 for data information).

similar to the range (0.26–1.0) given by McComiskey and Feingold (2008). It has been found, however, that satellite-retrieved values of $b(\log N_c)$ over the global ocean exist in a relatively narrow range, from 0.4–0.5, regardless of the data sources (i.e., AVHRR or MODIS). A large value from aircraft measurements (Kaufman et al. 1995) and a bin-type regional model result (Suzuki et al. 2006) suggest that a strong aerosol–cloud interaction is possible in a favorable condition of cloud nucleation, but insensitive cases (e.g., Leaitch et al. 1992) compensate for these large b values when a global mean is calculated using the tabulated values. Strongly differing values within one model, such as MIROC for various parameterizations (Suzuki et al. 2004) in Table 17.3, demonstrate that there is significant room for any model to be tuned so as to bring model results closer to the observed N_a–N_c relation.

LWP is related to CDR and COT in the following manner:

$$\mathrm{LWP} = 2\,\rho\,\mathrm{CDR} \times \mathrm{COT}/3, \tag{17.2}$$

where ρ is the density of water. This leads to a simple relation between the slopes for CDR and COT (Sekiguchi et al. 2003):

$$b(\log \mathrm{LWP}) = b(\log \mathrm{CDR}) + b(\log \mathrm{COT}). \tag{17.3}$$

Table 17.3 and Figure 17.6 show values of $b(\log \mathrm{CDR})$ and $b(\log \mathrm{LWP})$ reported by past studies, and values of $b(\log \mathrm{COT})$ can be calculated from Equation 17.3. Most satellite values correspond to water clouds, and it has been found that large differences exist among the reported values. This is understandable since the scatterplots from which the slopes have been derived tend to have extremely large dispersions, as reported in the past (e.g., Storelvmo et al. 2006). In our future work, this large dispersion will be studied. The preselection of one type of cloud as a target and a certain analysis method can also effect large differences in results; a serious problem for any satellite sensing lies in the fact

Chapter from:
Clouds in the Perturbed Climate System, edited by Jost Heintzenberg and Robert J. Charlson.
2009. Strüngmann Forum Report, vol. 2. Cambridge, MA: MIT Press. ISBN 978-0-262-01287-4

Source[1]	Data	*A*	$Y = \log \mathrm{CDR}$	log COT	log LWP	log N_c	CF	
(1)	aircraft	*Na*				0.700		
(2)	aircraft	*Na*				0.257		
(3)	POLDER	AI	–0.046					
(4)	MODIS	AOD	0.010	0.150	0.160		0.342*t*	
(5)	MODIS	AOD			0.051		0.244*w*	
(6)	GCM	*Na*				0.410		Globe
(3)	LMDZ	AI	–0.150					
(3)	LMDZ-fit	AI	–0.078					
(3)	LMDZ multi, fit	AI	–0.048					
(7)	AVHRR	*Na*	–0.094	0.257	0.163	0.500		
(8)	AVHRR	*Na*	–0.100	0.156	0.040	0.388	0.086*w*	
(9)	POLDER	AI	–0.078					
(8)	POLDER	*Na*	–0.069					
(10)	POLDER	AI	–0.044	0.203	0.159			
(11)	MODIS	AI	–0.244	0.036	–0.208			
(12)	MODIS	AOD-fine				0.384		
(4)	MODIS	AOD	–0.068	0.142	0.073		0.330*w*	
(5)	MODIS	AOD			0.042		0.299*w*	Global
(7)	Grantour	*Na*	–0.203			0.490		Ocean
(13)	MIROC, Berry	*Na*	–0.187	0.204	0.064			
(13)	MIROC, Khairoutdinov	*Na*	–0.103	0.262	0.227			
(13)	MIROC, Sundqvist	*Na*	–0.178	0.052	–0.104			
(10)	LMDZ	AI	–0.099	0.150	0.051			
(12)	LMDZ	AOD-fine				0.493		
(12)	ECHAM	AOD-fine				0.805		
(12)	LMDZ fit	AOD-fine				0.191		
(12)	ECHAM fit	AOD-fine				0.350		
(11)	GOCART	AI	–0.243	0.017	–0.226			

(10)	POLDER, 30°–60°N	AI			0.113			
(14)	MODIS, AO 30°–60°N	AOD	–0.046	0.069	0.023		0.121*w*	
(14)	MODIS, AO 5°–30°N	AOD	–0.046	0.081	0.035		0.271*w*	
(14)	MODIS, AO 20°S–5°N	AOD	–0.124	0.042	–0.081		0.293*w*	
(14)	MODIS, AO 30°–20°S	AOD	–0.174	0.309	0.135		0.238*w*	Regional Ocean
(4)	MODIS, AO 30°–60°N	AOD					0.445*t*	
(4)	MODIS, AO 5°–30°N	AOD					0.433*t*	
(4)	MODIS, AO 20°S–5°N	AOD					0.471*t*	
(4)	MODIS, AO 30°–20°S	AOD					0.457*t*	
(10)	LMDZ, 30–60°N	AI			0.078			
(15)	Regional bin model	*Na*	–0.373	0.330	–0.043	0.720		
(9)	POLDER	AI	–0.035					
(8)	POLDER	*Na*	–0.035					
(10)	POLDER	AI	0.003	0.032	0.035			Global Land
(4)	MODIS	AOD	0.079	0.157	0.236		0.352*t*	
(5)	MODIS	AOD			0.062		0.210*w*	
(10)	LMDZ	AI	–0.086	0.105	0.019			
(10)	POLDER, 30°–60°N	AI			0.221			
(10)	LMDZ, 30°–60°N	AI			0.146			Regional Land
(16)	Surface, China S, E & N	AOD					–0.054*t*	

Table 17.3 Slope *b* of the regression line between aerosol loading, *A*, and cloud parameter, $Y = a + b \log(A)$, reported by past studies. Listed regions for (1) and (4) are latitudinal zones of the Atlantic Ocean (AO). Underlined values were not reported originally, but are estimated by the relation of $b(\log \text{LWP}) = b(\log \text{CDR}) + b(\log \text{COT})$. Values of b(CF) in (5) were estimated from the b(log CF) and mean CF values of (4). The value in (16) is for the total cloud fraction change in the period of 1951–1994. AOD: aerosol optical depth; CDR: cloud droplet radius; COT: cloud optical thickness; LWP: liquid water path; N_c: cloud droplet number, *w* and *t* attached to values stand for water cloud fraction and total CF, respectively.

[1] (1) Kaufman et al. (1991), (2) Leaitch et al. (1992), (3) Quaas and Boucher (2005), (4) Myhre et al. (2007), (5) Quaas et al. (2008), (6) Boucher and Lohmann (1995), (7) Nakajima et al. (2001), (8) Sekiguchi et al. (2003), (9) Bréon et al. (2002), (10) Quaas et al. (2004), (11) Matsui et al. (2006), (12) Quaas et al. (2006), (13) Suzuki et al. (2004), (14) Kaufman et al. (2005), (15) Suzuki et al. (2006), (16) Mukai et al. (2008).

Chapter from:
Clouds in the Perturbed Climate System, edited by Jost Heintzenberg and Robert J. Charlson.
2009. Strüngmann Forum Report, vol. 2. Cambridge, MA: MIT Press. ISBN 978-0-262-01287-4

Chapter from:
Clouds in the Perturbed Climate System, edited by Jost Heintzenberg and Robert J. Charlson.
2009. Strüngmann Forum Report, vol. 2. Cambridge, MA: MIT Press. ISBN 978-0-262-01287-4

that aerosol and cloud information is derived from clear and cloudy pixels, respectively, which are different from each other both spatially and temporarily. Despite these difficulties, however, a decreasing trend of CDR with the aerosol loading has been found over the ocean and is relatively well simulated by models with a slight overestimation.

Over land, a neutral or a slight increasing trend in CDR is observed but is difficult to simulate. A simple Twomey mechanism is not enough to explain this phenomenon, as will be discussed later for the cloud fraction (CF) change. LWP seems to increase over both ocean and land, suggesting that there is a mechanism of the cloud lifetime effect (Albrecht 1989). Further modeling efforts are needed to simulate such an observed tendency. Changes of ECHAM cloud and aerosol schemes lead to –1.9 Wm^{-2}, whereas former versions of ECHAM produce values of –1.0 Wm^{-2} to –2.6 Wm^{-2} for the simulated indirect effect (Table 3 in Lohmann et al. 2007). Suzuki et al. (2004) obtained a large negative slope b(log LWP) when the lifetime effect is eliminated from the model by introducing the Sundqvist parameterization ($p = 0$) of the autoconversion rate, $\tau_p \propto Nc^p$, for the cloud to precipitation conversion process. This is because aerosols tend to accumulate in high-pressure areas where a less than average amount of clouds are present. Inclusion of the lifetime effect by Berry's ($p = 1$) or Khairoutdinov's ($p = 1.79$) parameterization makes the system produce more LWP through the cloud lifetime effect. It should be recognized that the cloud lifetime effect makes the LWP insensitive to particle concentrations by

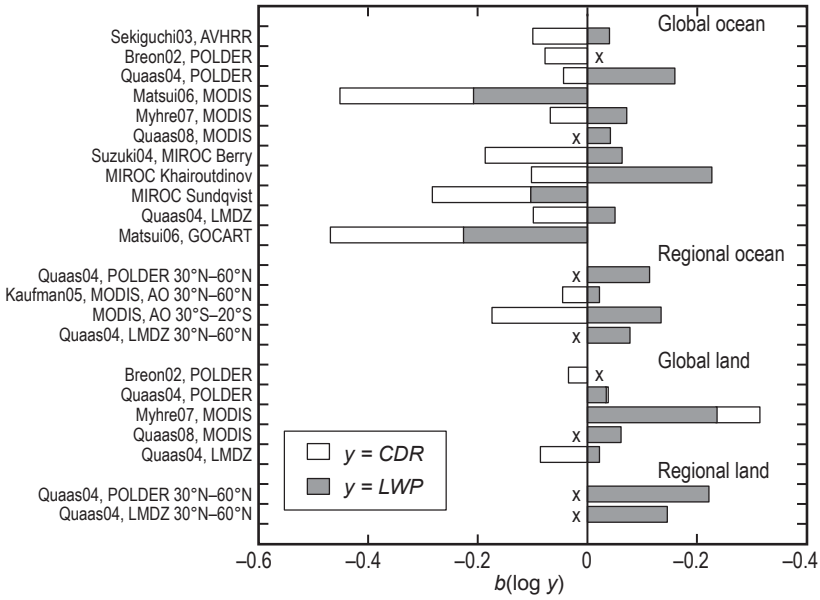

Figure 17.6 Reported values of the regression slope b(log CDR) and b(log LWP). Data labeled "x" have only one LWP or CDR slope.

Chapter from:
Clouds in the Perturbed Climate System, edited by Jost Heintzenberg and Robert J. Charlson.
2009. Strüngmann Forum Report, vol. 2. Cambridge, MA: MIT Press. ISBN 978-0-262-01287-4

canceling the large negative slope in the case of no aerosol–cloud interaction in the autoconversion process by the Sundqvist parameterization. Figure 17.6 suggests a suitable p value exists around 1–1.79, since satellite values over global ocean range from 0.04–0.163 for b(log LWP) other than a large negative value of Matsui et al. (2006), whereas the model result of Suzuki et al. (2004) ranges from 0.064 (for $p = 1$) to 0.227 ($p = 1.79$), respectively. More validation and cloud microphysical modeling is needed, however, to confirm this point. The large negative value by Matsui et al. (2006) was obtained for low clouds with the cloud-top temperature above 273 K. They suggest two possible mechanisms of reduced LWP for such warm clouds under high aerosol loading condition: (a) enhanced evaporation of cloud droplets by light absorption of aerosols and/or by reduced cloud droplet size; (b) a change in the atmospheric stability by drizzle quenching to reduce water supply from the cloud bottom. These mechanisms are diffucult to implement explicitly in GCMs. It is also shown that the difference in target clouds is significant for comparison of the statistics.

Cloud Fraction Change

Cloud fraction can also be altered by aerosol effects. Figure 17.7 shows reported values of the slope of the following regression:

$$\mathrm{CF} = a(\mathrm{CF}) + b(\mathrm{CF}) \log(A). \tag{17.4}$$

In using this, we note that the relation may include an error caused by aerosol-containing pixels when the relative humidity is high. Another important point is that some studies use the water CF whereas others use the total CF for the analysis. In case middle- and upper-layer clouds do not respond to A, the slope b(CF) for water clouds will be similar to that for total clouds, although there are case studies that suggest this assumption is questionable (cf. Figure 17.10).

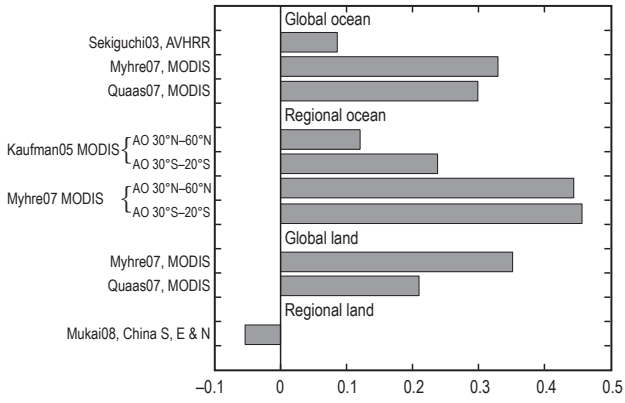

Figure 17.7 Reported values of the regression slope b(CF).

Chapter from:
Clouds in the Perturbed Climate System, edited by Jost Heintzenberg and Robert J. Charlson.
2009. Strüngmann Forum Report, vol. 2. Cambridge, MA: MIT Press. ISBN 978-0-262-01287-4

All measurements shown in Figure 17.7 suggest an increasing trend of the CF over the ocean, but there is a large difference between 0.086 by Sekiguchi et al. (2003) and 0.35 by Myhre et al. (2007) and Quaas et al. (2008). Kaufman et al. (2005) reported a significant increase of CF of shallow water clouds with increasing aerosol concentrations that produces an aerosol indirect RF larger than those by first and second indirect effects over the Atlantic Ocean. Myhre et al. (2007) reported a similar analysis for the same regions, but for the total CF, and obtained stronger CF changes than those obtained by Kaufman et al. (2005). Thus, more investigations are needed to identify the causes of the different cloud types. It is interesting to note that clouds over land have globally a positive slope compared to the ocean values. This indicates a significant increase in the large area mean of CF with increasing aerosol concentrations, despite several reports which suggest decreases of the CF attributable to aerosols over some regions (Kaiser 2000; Koren et al. 2004), also shown by the value given by Mukai et al. (2008) for the Chinese region.

Various Indirect Effects of Aerosols

As many researchers have suggested, the cloud field is influenced not only by first and second aerosol indirect effects but also by other processes, such as an atmospheric stability. Matsui et al. (2005, 2006) found that the drizzle particle growth in low-level clouds can be classified by AI and the lower tropospheric stability. In Figure 17.8 we compare their distribution of precipitating/non-precipitating clouds and b(log CDR) of Sekiguchi et al. (2003). The figure indicates that areas of large negative b-values tend to correspond to the location of non-precipitating clouds without much drizzling particles. On the other hand, regions of neutral to positive b(log CDR) values exist in regions with precipitating clouds, which also coincide with strongly active convective regions like ITCZ or SPCZ. This suggests that to simulate b-values better, it is important to model the drizzle-forming or suppression processes in conjunction with the nucleation process and large-scale dynamics that control lower tropospheric stability. High-resolution and bin-type aerosol–cloud particle growth models should be useful for such studies.

Figure 17.9 shows two characteristic COT-CDR scatterplots from AVHRR, which have been observed frequently off the Californian coast and over the North Atlantic (Nakajima and Nakajima 1995). Here, we present corresponding simulation results by a bin-type non-hydrostatic cloud model for low and high CCN conditions (Suzuki et al. 2006). The model successfully simulates the characteristic negative correlation between COT and CDR in the pristine condition with abundant drizzle particles by which the COT decreases when CDR becomes large. For the polluted case, there tends to be a positive correlation between COT and CDR because the COT increases when drizzling is quenched by reduced CDR with increasing CCN. Hence the large negative

Chapter from:
Clouds in the Perturbed Climate System, edited by Jost Heintzenberg and Robert J. Charlson.
2009. Strüngmann Forum Report, vol. 2. Cambridge, MA: MIT Press. ISBN 978-0-262-01287-4

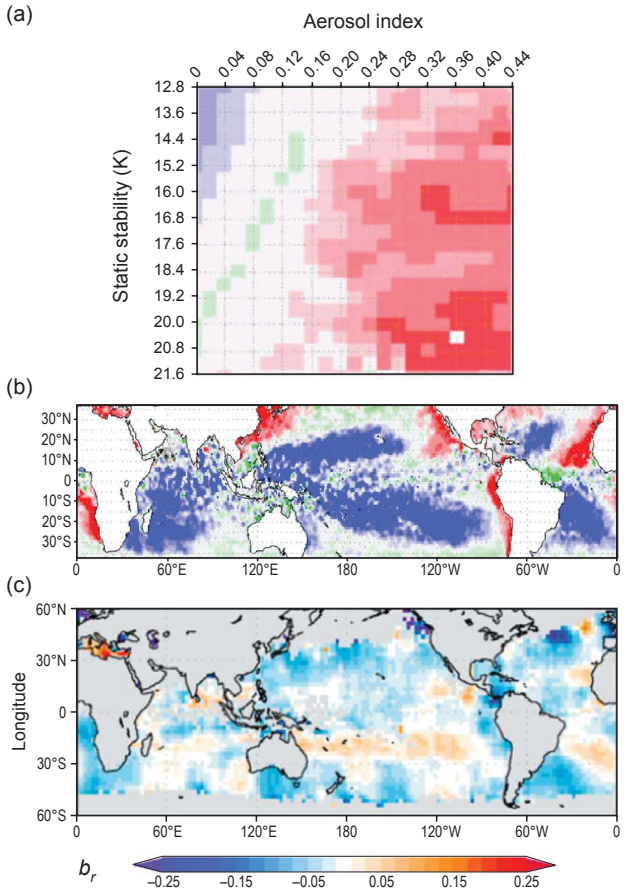

Figure 17.8 Classification of precipitating/non-precipitating clouds from a combined visible and microwave remote sensing (a) and their global distribution for March–June 2000 (after Fig. 3a in Matsui et al. 2004); (b) data from Matsui et al. (2004) is compared with *b*(log CDR) for April, 1990 (after fig. 5 in Matsui et al. 2004); (c) data from Sekiguchi et al. (2003). Red, green, and blue in (a) and (b) indicate non-precipitating, neutral, and precipitating clouds, respectively.

b(log CDR) values in these regions are produced by a drizzle-quenching mechanism that results from CCN input.

In terms of the cloud stratification, it is interesting to study how cloud-top temperature depends on aerosol parameters. Sekiguchi et al. (2003) found the *T14*-temperature, at which CDR exceeds 14 μm (Rosenfeld 2000), decreases with N_a, but they did not find a significant dependence of the cloud-top temperature on N_a. This result looks reasonable because the particle growth is delayed when CCN are added to the cloud system, whereas the cloud-top height is rather controlled by large-scale dynamics. However, Myhre et al. (2007) reported a significant positive correlation between the cloud-top pressure and

Chapter from:
Clouds in the Perturbed Climate System, edited by Jost Heintzenberg and Robert J. Charlson.
2009. Strüngmann Forum Report, vol. 2. Cambridge, MA: MIT Press. ISBN 978-0-262-01287-4

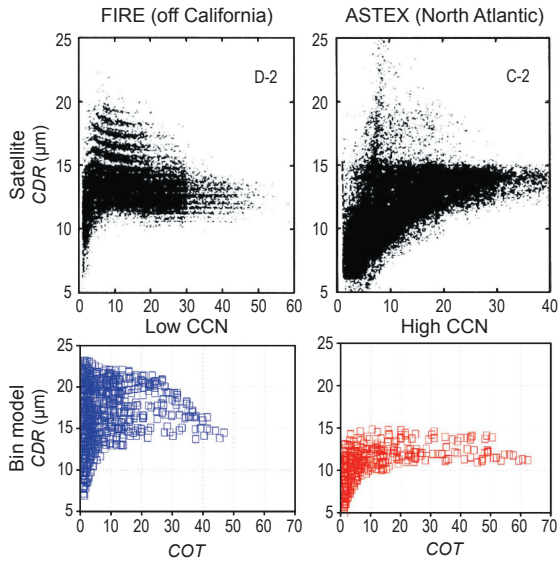

Figure 17.9 COT–CDR correlations from satellite (Nakajima and Nakajima 1995) and a bin-type cloud model (Suzuki et al. 2006) for FIRE and ASTEX experiments.

AOD. Further investigations are needed to resolve the differences in target clouds used in these studies.

Lohmann et al. (2006) point out that high and low AOD cases correspond to very different atmospheric conditions. In addition, a secondary general circulation is induced by a large-scale aerosol direct forcing, which cools the Earth's surface and heats the atmosphere (Menon et al. 2002; Chuang and Ramanathan 2006, 2007; Takemura et al. 2005, 2007). A complication of these mechanisms associated with atmospheric dynamics is that clouds are under the influence of both anthropogenic aerosols and greenhouse gases. Unraveling the mechanisms of cloud change is thus not a simple task, because an increase in anthropogenic aerosols is correlated with an increase in anthropogenic greenhouse gas concentrations. Figure 17.10 demonstrates long-term, surface-observed changes in the total CF from the World Surface Observation data (Japan Meteorological Business Support Center) from 1951–1994 as well as simulated CF changes in three regions of China (Mukai et al. 2008). The simulation results show differences between equilibrium experiments of the MIROC+SPRINTARS model, coupled with a mixed ocean, for preindustrial conditions and for current anthropogenic aerosols (AER), greenhouse gases (GHG), and the combination of both (AER+GHG). Thus the magnitude of the change should not be used for quantitative comparison with observed changes. Figure 17.10 suggests that the large CF increase attributable to the aerosol effect is mostly negated in the model simulation by the CF decrease as a result of the GHG effect in the eastern (E) and northern (N) regions. By comparison, the

Chapter from:
Clouds in the Perturbed Climate System, edited by Jost Heintzenberg and Robert J. Charlson.
2009. Strüngmann Forum Report, vol. 2. Cambridge, MA: MIT Press. ISBN 978-0-262-01287-4

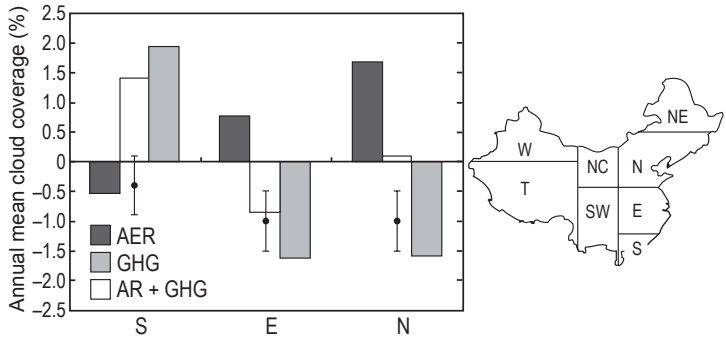

Figure 17.10 Simulated changes in the annual mean cloud coverage (%) attributable to anthropogenic aerosols (AER), greenhouse gases (GHG), and both (AER+GHG) over three Chinese regions: S, E, and N. Closed circles with standard error bar represent the changes in the observed cloud coverage (%) from 1951–1994 (data from Mukai et al. 2008).

southern (S) region exhibits increase/decrease trends that are almost opposite to those of regions E and N. A further complication is that the CF decrease in region S is caused by a decrease in the convective CF, which exceeds the increase of low CF produced by the cloud lifetime effect of anthropogenic aerosols in this region. This large decrease of the convective CF is the result of an enhanced anti-cyclonic circulation caused by the enhanced atmospheric stability and land–ocean temperature gradient, which are, in turn, caused by the large negative aerosol RF at the surface. Convective clouds increase in region N through the counter-circulation of the region S. Thus the change of the total CF, including all types of clouds, results from a very complicated mechanism over this region, as suggested partly (remember that satellite values are mostly for water clouds) by a poor model simulation of *b*(log CDR) and *b*(log LWP) changes over the global land (see Figure 17.6). In addition, the areal mean of the CF change over China becomes very small (< 10 %), much smaller than the large-area averages estimated by satellites. Thus, we need to understand how such a small change in total CF from long-term surface observations and a large change in CF from satellite data can occur, if we are to exact a global understanding of perturbed clouds.

Conclusions and Recommendations

Columnar anthropogenic aerosol amounts and their RF are captured in some detail by observations from space and surface. Model estimates of total AOD are within a range of 0.05 of sun photometer and satellite retrieval estimates (Kinne et al. 2006). Global-scale features of the aerosol–cloud interaction are also estimated from observations and are well simulated by models over the ocean, but perturbed clouds over the land seem to be more difficult to simulate.

Chapter from:
Clouds in the Perturbed Climate System, edited by Jost Heintzenberg and Robert J. Charlson.
2009. Strüngmann Forum Report, vol. 2. Cambridge, MA: MIT Press. ISBN 978-0-262-01287-4

Dimming and brightening by aerosol particles have been suggested to alter the surface solar radiation on decadal scales regionally by several W m^{-2}. This perturbation of the regional surface radiation budget seems to have caused noticeable large-scale cloud field changes.

To address the open issues, we recommend the following research efforts:

- Aerosol properties, especially the mixing state of soot particles, should be measured more thoroughly because the anthropogenic AOD and the clear-sky forcing efficiency are smaller in the models than retrieved from observations. The regional aerosol effect and the aerosol-induced perturbation of the vertical structure of the atmosphere depend critically on particulate absorption.
- Active remote measurements should be combined with passive sensing to reduce the difficulty in obtaining simultaneous aerosol and cloud measurements to derive the aerosol–cloud interaction strength. CloudSat, CALIPSO, and future EarthCARE platforms offer a unique opportunity to improve our understanding of these processes. Passive satellite sensors cannot alone discriminate well enough the location in the column aerosol where clouds are actually in the process of being mixed.
- Global climate modeling needs to include more elaborate aerosol and cloud microphysical processes to simulate various aerosol and cloud processes, including large-scale dynamic–hydrologic effects. High-resolution modeling may help us understand continental and convective clouds without the simplifying cumulus parameterizations that have been used in global climate models. At the same time, such simulations require more thorough testing with benchmark datasets to determine the quality of model descriptions of critical processes. The nature of most of the aerosol observations prevents a direct identification of the anthropogenic contributions. In many regions, natural aerosols dominate particulate mass, AOD, and often CCN concentrations as well. Therefore, natural aerosols require as much attention as anthropogenic aerosols when investigating the anthropogenic perturbations of the cloud system.
- Our understanding of long-term trends of atmospheric aerosol concentrations and thus the anthropogenic perturbation is incomplete. Further efforts are required to characterize sufficiently pristine and anthropogenic aerosol levels, and we recommend that this be done by integrating results from different methods. A conceptual or even quantitative model of the temporal and regional evolution of particle composition and CCN concentrations may be helpful to investigate the anthropogenic perturbation of clouds.

Chapter from:
Clouds in the Perturbed Climate System, edited by Jost Heintzenberg and Robert J. Charlson.
2009. Strüngmann Forum Report, vol. 2. Cambridge, MA: MIT Press. ISBN 978-0-262-01287-4

Acknowledgments

Figure 17.4 was kindly provided by NASA MODIS team, Takashi Y. Nakajima and Toshihiko Takemura. Model results of anthropogenic aerosol properties have been made accessible thanks to the AeroCom project partners: Olivier Boucher, Shekar Reddy, Philip Stier, Toshihiko Takemura, Gunnar Myhre, Joyce Penner, and Xhiaohong Liu.

References

Albrecht, B. A. 1989. Aerosols, cloud microphysics, and fractional cloudiness. *Science* **245**:1227–1230.

Andreae, M. O. 2007. Aerosols before pollution. *Science* **315(5808)**:50–51.

Bellouin, N., O. Boucher, J. Haywood, and M. S. Reddy. 2005. Global estimate of aerosol direct radiative forcing from satellite measurements. *Nature* **438(7071)**:1138–1141.

Boucher, O., and U. Lohmann. 1995. The sulfate-CCN-cloud albedo effect: A sensitivity study with two general circulation models. *Tellus B* **47**:281–300.

Boucher, O., and M. Pham. 2002. History of sulfate aerosol radiative forcings. *Geophys. Res. Lett.* **29(9)**:22–25.

Bréon, F. -M., D. Tanré, and S. Generoso. 2002. Aerosol effect on cloud droplet size monitored from satellite. *Science* **295**:834–837.

Chameides, W. L., C. Luo, R. Saylor et al. 2002. Correlation between model-calculated anthropogenic aerosols and satellite-derived cloud optical depths: Indication of indirect effect. *J. Geophys. Res.* **107**:4085.

Chung, C. E., and V. Ramanathan. 2006. Weakening of North Indian SST Gradients and the Monsoon Rainfall in India and the Sahel. *J. Climate* **19**:2036.

Chung, C. E., and V. Ramanathan. 2007. Relationship between trends in land precipitation and tropical SST gradient. *Geophys. Res. Lett.* **34**:L16809.

Chung, C. E., V. Ramanathan, D. Kim, and I. A. Podgorny. 2005. Global anthropogenic aerosol direct forcing derived from satellite and ground-based observations. *J. Geophys. Res.* **110**:D24207.

Coakley, J. A., Jr., R. L. Bernstein, and P. A. Durkee. 1987. Effect of ship-track effluents on cloud reflectivity. *Science* **237**:1020–1022.

Forster, P., V. Ramaswamy, Artaxo et al. 2007. Radiative Forcing of Climate Change. In: Climate Change 2007: The Physical Science Basis. Contribution of Working Group I to the Fourth Assessment Report of the Intergovernmental Panel on Climate Change, edited by S. Solomon, D. Qin, M. Manning et al. pp. 129–234. New York. Cambridge Univ. Press.

Goto-Azuma, K., and R. M. Koerner. 2001. Ice core studies of anthropogenic sulfate and nitrate trends in the Arctic. *J. Geophys. Res. Atmos.* **106(D5)**:4959–4969.

Han, Q., W. B. Rossow, and A. A. Lacis. 1994. Near-global survey of effective droplet radii in liquid water clouds using ISCCP data. *J. Climate* **7**:465–497.

Haywood, J., and M. Schulz. 2007. Causes of the reduction in uncertainty in the anthropogenic radiative forcing of climate between IPCC (2001) and IPCC (2007). *Geophys. Res. Lett.* **34(20)**:L20701.

Heidam, N. Z., J. Christensen, P. Wahlin, and H. Skov. 2004. Arctic atmospheric contaminants in NE Greenland: levels, variations, origins, transport, transformations and trends 1990–2001. *Sci. Environ.* **331(1–3)**:5–28.

Chapter from:
Clouds in the Perturbed Climate System, edited by Jost Heintzenberg and Robert J. Charlson.
2009. Strüngmann Forum Report, vol. 2. Cambridge, MA: MIT Press. ISBN 978-0-262-01287-4

Kaiser, D. P. 2000. Decreasing cloudiness over China: An updated analysis examining additional variables. *Geophys. Res. Lett.* **27**:2193–2196.

Kaufman, Y. J., O. Boucher, D. Tanré et al. 2005. Aerosol anthropogenic component estimated from satellite data. *Geophys. Res. Lett.* **32(17)**:L17804.

Kaufman, Y. J., R. S. Fraser, and R. L. Mahoney. 1991. Fossil fuel and biomass burning effect on climate: Heating or cooling? *J. Climate* **4**:578–588.

Kaufman, Y. J., I. Koren, L. A. Remer, D. Rosenfeld, and Y. Rudich. 2005. The effect of smoke, dust, and pollution aerosol on shallow cloud development over the Atlantic Ocean. *PNAS* **102**:11,207–11,212.

Kawamoto, K., T. Hayasaka, T. Nakajima, D. Streets, and J.-H. Woo. 2004. Examining the aerosol indirect effect using SO_2 emission inventory over China using SO_2 emission inventory. *Atmos. Res.* **72**:353–363.

Kawamoto, K., T. Hayasaka, I. Uno, and T. Ohara. 2006. A correlative study on the relationship between modeled anthropogenic aerosol concentration and satellite-observed cloud properties over East Asia. *J. Geophys. Res.* **111**:D19201.

Kawamoto, K., and T. Nakajima. 2003. Seasonal variation of cloud particle size as derived from AVHRR remote sensing. *Geophys. Res. Lett.* **30**:1810.

Kawamoto, K., T. Nakajima, and T. Y. Nakajima. 2001. A global determination of cloud microphysics with AVHRR remote sensing. *J. Climate* **14**:2054–2068.

King, M. D., Y. J. Kaufman, D. Tanré, and T. Nakajima. 1999. Remote sensing of tropospheric aerosols from space: Past, present, and future. *Bull. Amer. Meteor. Soc.* **80**:2229–2259.

Kinne, S., M. Schulz, C. Textor et al. 2006. An AeroCom initial assessment optical properties in aerosol component modules of global models. *Atmos. Chem. Phys.* **6**:1815–1834.

Koren, I., Y. J. Kaufman, L. A. Remer, and J. V. Martins. 2004. Measurement of the effect of Amazon smoke on inhibition of cloud formation. *Science* **303**:1342–1345.

Leaitch, W. R., G. A. Isaac, J. W. Strapp, C. M. Banic, and H. A. Wiebe. 1992. The relationship between cloud droplet number concentrations and anthropogenic pollution: Observation and climatic implications. *J. Geophys. Res.* **97**:2463–2474.

Legrand, M., C. Hammer, M. DeAngelis et al. 1997. Sulfur-containing species (methanesulfonate and SO_4) over the last climatic cycle in the Greenland Ice Core Project (central Greenland) ice core. *J. Geophys. Res. Ocean.* **102(C12)**:26,663–26,679.

Liepert, B., and I. Tegen. 2002. Multidecadal solar radiation trends in the United States and Germany and direct tropospheric aerosol forcing. *J. Geophys. Res. Atmos.* **107(D12)**:4153.

Lohmann, U., I. Koren, and Y. J. Kaufman. 2006. Disentangling the role of microphysical and dynamical effects in determining cloud properties over the Atlantic. *Geophys. Res. Lett.* **33**:L09802.

Lohmann, U., P. Stier, C. Hoose et al. 2007. Cloud microphysics and aerosol indirect effects in the global climate model ECHAM5-HAM. *Atmos. Chem. Phys.* **7**:3425−3446.

Matsui, T., H. Masunaga, S. M. Kreidenweis et al. 2006. Satellite-based assessment of marine low cloud variability associated with aerosol, atmospheric stability, and the diurnal cycle. *J. Geophys. Res.* **111**:D17204.

Matsui, T., H. Masunaga, R. A. Pielke, Sr., and W.-K. Tao. 2004. Impact of aerosols and atmospheric thermodynamics on cloud properties within the climate system. *Geophys. Res. Lett.* **31**:L06109.

McComiskey, A., and G. Feingold.2008. Quantifying error in the radiative forcing of the first aerosol indirect effect. *Geophys. Res. Lett.* **35**:L02810.

Chapter from:
Clouds in the Perturbed Climate System, edited by Jost Heintzenberg and Robert J. Charlson.
2009. Strüngmann Forum Report, vol. 2. Cambridge, MA: MIT Press. ISBN 978-0-262-01287-4

McConnell, J. R., R. Edwards, G.L. Kok et al. 2007. 20th-century industrial black carbon emissions altered arctic climate forcing. *Science* **317(5843)**:1381–1384.

Menon, S., J. Hansen, L. Nazarenko, and Y. Luo. 2002. Climate effects of black carbon aerosols in China and India. *Science* **297**:2250–2253.

Mishchenko, M. I., I. V. Geogdzhayev, B. Cairns et al. 2007a. Past, present, and future of global aerosol climatologies derived from satellite observations: A perspective. *J. Quant. Spectrosc. Rad. Trans.* **106(1–3)**:325–347.

Mishchenko, M. I., I. V. Geogdzhayev, W. B. Rossow et al. 2007b Long-term satellite record reveals likely recent aerosol trend. *Science* **315(5818)**:1543–1543.

Mukai, M., T. Nakajima, and T. Takemura. 2008. A study of anthropogenic impacts on the radiation budget and the cloud field in East Asia. *J. Geophys. Res.* **113**:D12211.

Myhre, G., F. Stordal, M. Johnsrud et al. 2007. Aerosol–cloud interaction inferred from MODIS satellite data and global aerosol models. *Atmos. Chem. Phys.* **7**:3081–3101.

Nakajima, T., A. Higurashi, K. Kawamoto, and J. E. Penner. 2001. A possible correlation between satellite-derived cloud and aerosol microphysical parameters. *Geophys. Res. Lett.* **28**:1171–1174.

Nakajima, T., M. D. King, J. D. Spinhirne, and L.F. Radke. 1991. Determination of the optical thickness and effective radius of clouds from reflected solar radiation measurements. Part II: Marine stratocumulus observations. *J. Atmos. Sci.* **48**:728–750.

Nakajima, T. Y., and T. Nakajima. 1995. Wide-area determination of cloud microphysical properties from NOAA AVHRR measurements for FIRE and ASTEX regions. *J. Atmos. Sci.* **52**:4043–4059.

Preunkert, S., M. Legrand, and D. Wagenbach. 2001. Sulfate trends in a Col du Dome (French Alps) ice core: A record of anthropogenic sulfate levels in the European midtroposphere over the twentieth century. *J. Geophys. Res. Atmos.* **106(D23)**:31,991–32,004.

Quaas, J., and O. Boucher. 2005. Constraining the first aerosol indirect radiative forcing in the LMDZ GCM using POLDER and MODIS satellite data. *Geophys. Res. Lett.* **32**:L17814.

Quaas, J., O. Boucher, N. Bellouin, and S. Kinne. 2008. Satellite-based estimate of the direct and indirect aerosol climate forcing. *J. Geophys. Res.* **113**:D05204.

Quaas, J., O. Boucher, and F.-M. Bréon. 2004. Aerosol indirect effects in POLDER satellite data and in the LMDZ GCM. *J. Geophys. Res.* **109**:D08205.

Quaas, J., O. Boucher, and U. Lohmann. 2006. Constraining the total aerosol indirect effect in the LMDZ and ECHAM4 GCMs using MODIS satellite data. *Atmos. Chem. Phys.* **6**:947–955.

Quinn, P. K., G. Shaw, E. Andrews et al. 2007. Arctic haze: Current trends and knowledge gaps. *Tellus* **59(1)**:99–114.

Radke, L. F., J. A. Coakley, Jr., and M. D. King. 1989. Direct and remote sensing observations of the effects of ships on clouds. *Science* **246**:1146–1149.

Ramanathan, V., M. V. Ramana, G. Roberts et al. 2007. Warming trends in Asia amplified by brown cloud solar absorption. *Nature* **448(7153)**:575–578.

Richter, A., J. P. Burrows, H. Nuss, C. Granier, and U. Niemeier. 2005. Increase in tropospheric nitrogen dioxide over China observed from space. *Nature* **437(7055)**:129–132.

Rosenfeld, D. 2000. Suppression of rain and snow by urban and industrial air pollution. *Science* **287**:1793–1796.

Chapter from:
Clouds in the Perturbed Climate System, edited by Jost Heintzenberg and Robert J. Charlson.
2009. Strüngmann Forum Report, vol. 2. Cambridge, MA: MIT Press. ISBN 978-0-262-01287-4

Schulz, M., C. Textor, S. Kinne et al. 2006. Radiative forcing by aerosols as derived from the AeroCom present-day and preindustrial simulations. *Atmos. Chem. Phys.* **6**:5225–5246.

Sekiguchi, M., T. Nakajima, K. Suzuki et al. 2003. A study of the direct and indirect effects of aerosols using global satellite datasets of aerosol and cloud parameters. *J. Geophys. Res.* **108(D22)**:4699.

Storelvmo, T., J. E. Kristjánsson, G. Myhre1, M. Johnsrud, and F. Stordal. 2006. Combined observational and modeling based study of the aerosol indirect effect. *Atmos. Chem. Phys.* **6**:3583–3601.

Suzuki, K., T. Nakajima, T. Y. Nakajima, and A. Khain. 2006. Correlation pattern between effective radius and optical thickness of water clouds simulated by a spectral bin microphysics cloud model. *SOLA* **2**:116–119.

Suzuki, K., T. Nakajima, A. Numaguti et al. 2004. A study of the aerosol effect on a cloud field with simultaneous use of GCM modeling and satellite observation. *J. Atmos. Sci.* **61**:179–194.

Takemura, T., Y. J. Kaufman, L. A. Remer, and T. Nakajima. 2007. Two competing pathways of aerosol effects on cloud and precipitation formation. *Geophys. Res. Lett.* **34**:L04802.

Takemura, T., T. Nozawa, S. Emori, T. Y. Nakajima, and T. Nakajima. 2005. Simulation of climate response to aerosol direct and indirect effects with aerosol transport-radiation model. *J. Geophys. Res.* **110**:D02202.

Takemura, T., Y. Tsushima, T. Yokohata et al. 2006. Time evolutions of various radiative forcings for the past 150 years estimated by a general circulation model. *Geophys. Res. Lett.* **33**:LI9705.

Wild, M., H. Gilgen, A. Roesch et al. 2005. From dimming to brightening: Decadal changes in solar radiation at Earth's surface. *Science* **308(5723)**:847–850.

Yu, H., Y. J. Kaufman, M. Chin et al. 2006. A review of measurement-based assessment of aerosol direct radiative effect and forcing. *Atmos. Chem. Phys.* **5**:613–666.

Chapter from:
Clouds in the Perturbed Climate System, edited by Jost Heintzenberg and Robert J. Charlson.
2009. Strüngmann Forum Report, vol. 2. Cambridge, MA: MIT Press. ISBN 978-0-262-01287-4

Chapter from:
Clouds in the Perturbed Climate System, edited by Jost Heintzenberg and Robert J. Charlson.
2009. Strüngmann Forum Report, vol. 2. Cambridge, MA: MIT Press. ISBN 978-0-262-01287-4